

No Data? No Problem: Robust Vision-Tabular Learning with Missing Values

Marta Hasny^{1,2} Laura Daza^{1,2} Keno Bressemer¹ Maxime Di Folco^{1,2} Julia Schnabel^{1,2,3}

¹ Technical University of Munich ² Helmholtz Munich ³ King’s College London

Abstract

Large-scale medical biobanks provide imaging data complemented by extensive tabular information, such as demographics or clinical measurements. However, this abundance of tabular attributes does not reflect real-world datasets, where only a subset of attributes may be available. This discrepancy calls for methods that can leverage all the tabular data during training while remaining robust to missing values at inference. To address this challenge, we propose RoVTL (Robust Vision-Tabular Learning), a framework designed to handle any level of tabular data availability, from 0% to 100%. RoVTL comprises two key stages: contrastive pre-training, where we introduce tabular attribute missingness as data augmentation to promote robustness, and downstream task tuning using a gated cross-attention module for multimodal fusion. During fine-tuning, we employ a novel Tabular More vs. Fewer loss that ranks performance based on the amount of available tabular data. Combined with disentangled gradient learning, this enables consistent performance across all tabular data completeness scenarios. We evaluate RoVTL on cardiac MRI scans from the UK Biobank, demonstrating superior robustness to missing tabular data compared to prior methods. Furthermore, RoVTL successfully generalizes to an external cardiac MRI dataset for multimodal disease classification, and extends to the natural images domain, achieving robust performance on a car advertisements dataset. The code is available at <https://github.com/marteczkah/RoVTL>.

1. Introduction

Tables provide a structured way to represent diverse types of information, ranging from categorical to continuous variables, and thus capture aspects that are often not visible in images. When combined, tabular and imaging data offer complementary views: images encode spatial and morphological patterns, while tables provide contextual information. A valuable source of such multimodal data are large population studies, such as the UK Biobank [27] and the German National Cohort [11], which pair extensive tabular informa-

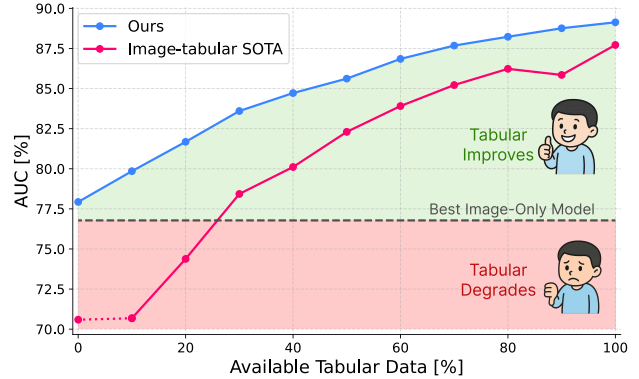


Figure 1. RoVTL consistently outperforms image-only inference [15] and prior multimodal baselines [6], addressing their key limitation of degraded performance in realistic clinical scenarios where less than 30% of tabular entries are available. The dotted line indicates an edge case evaluated in our work but absent from the original paper [6].

tion with imaging data suitable for training vision–tabular models. However, even such studies frequently contain missing tabular entries, as complete data cannot always be collected from every participant. Furthermore, in real-world settings, it is often impractical to collect the same amount of tabular attributes [10], making it difficult to deploy models trained on those extensive datasets. This gap highlights the need for methods that can leverage the rich tabular information available during training while remaining robust when only limited or no tabular data are available.

Previous works have addressed those issues using two main approaches. The first, exemplified by MMCL [13] and TGV [15], leverages images and tabular data during pretraining to create a joint representation space, but relies solely on images for downstream tuning and prediction. This strategy addresses uncertainty of tabular data availability at inference. However, because not all tabular attributes have visual counterparts, valuable complementary information may be overlooked. The second strategy, adopted by methods such as TIP [6], incorporates both image and tabular data during pretraining and inference, even when tabular entries

are missing. However, this approach has not been evaluated in the extreme case where tabular data is absent, nor has it been tested on external datasets, due to the rigid design of its tabular encoder. As a result, existing vision-tabular methods are typically designed for either image-only or joint image-tabular inference, without supporting both scenarios. However, in real-world settings, subjects may have complete, partial, or entirely missing tabular data. As shown in Fig. 1, this limited design of existing methods results in tabular data not always improving or even harming performance compared to image-only models.

To address the heterogeneous nature of tabular data, recent advances in tabular foundation models have introduced flexible tabular encoders capable of handling diverse column semantics. One such model is TARTE [20], which leverages a language model to represent both column names and categorical values, capturing the underlying semantics of each feature. This semantic embedding approach produces consistent and meaningful representations that generalize well across heterogeneous tables and does not require all attributes to be present. However, these representations are not integrated with visual features.

Building on these advances, we introduce RoVTL, **Robust Vision-Tabular Learning**, designed to deliver consistent performance across varying levels of tabular data availability. RoVTL maintains strong image-only capability while effectively leveraging tabular data when present. Our method is composed of two main steps: (1) We employ multimodal contrastive pretraining to learn vision and tabular encoders, introducing *data missingness* as an augmentation strategy to improve robustness to incomplete tabular inputs. (2) We fuse multimodal features through a gated cross-attention mechanism that adaptively controls the influence of tabular data on the joint embeddings. To handle missing tabular entries, we propose the Tabular More vs. Fewer loss (TabMoFe), which adapts the More vs. Fewer loss [22], originally designed for missing modalities, to address incomplete tabular attributes. We incorporate disentangled gradient learning (DGL) [30] to ensure effective optimization of the encoders during downstream training.

We conduct extensive experiments to evaluate the effectiveness of our proposed method on both classification and regression tasks across varying tabular data completeness scenarios. Specifically, we use cardiac MR images and clinical data from the UK Biobank [27] to assess performance on the challenging tasks of cardiovascular artery disease (CAD) classification and body mass index (BMI) regression. To examine the generalizability of our pretrained encoders, we further evaluate cardiac disease classification on a public external dataset [4]. In addition, we demonstrate that our framework seamlessly transfers to non-medical domains by evaluating it on a car advertisements dataset [18], showing its adaptability to natural vision-tabular settings.

In summary, our contributions are as follows. (1) We are the first to propose a method addressing the full spectrum of tabular data missingness, ranging from no to complete tabular data. (2) We introduce RoVTL, featuring a novel data missingness augmentation approach and an effective downstream task fine-tuning strategy, involving TabMoFe loss and DGL. (3) Experiments on medical and natural images datasets show that RoVTL surpasses the SOTA methods across varying tabular data availability scenarios, scoring the highest improvement when little tabular data is available. (4) We show generalization to external cardiac and natural domain datasets, highlighting potential for vision-tabular foundation models.

2. Related Works

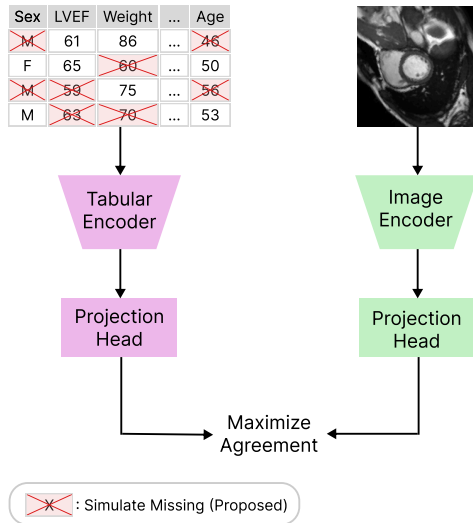
2.1. Learning with Tabular Data

Tabular data is a common modality in many disciplines, including finance and medicine. Traditional machine learning methods, such as decision tree models like XGBoost [5], achieve great performance on tabular data tasks that deep learning have struggled to surpass [12]. While successful in unimodal setting, these models do not provide the capability to be used multimodally. In recent years, deep learning models, particularly those based on the transformer architecture [29], have started to rival and even outperform tree-based methods on sufficiently large datasets [32]. Furthermore, the success of vision [1] and language foundation models [33] has spurred interest in developing similar foundation models for tabular data. Models such as TabICL [24] and TabPFN [17] represent important advancements toward tabular foundation models. However, those models are often designed for a single task, which limits their scope and flexibility compared to foundation models in other domains, such as language and vision. TARTE [20] addresses these limitations by leveraging large knowledge bases for pretraining and encoding feature semantics through string representations. By providing a general and transferable architecture, this design enables a tabular foundation model that could align with vision and language counterparts, opening possibilities for effective multimodal learning with tabular data. We exploit this capability in our method.

2.2. Image-Tabular Data Learning.

End-to-End Approaches. Tabular data can improve visual learning by bringing complementary information that is not visible in the images, motivating the development of multimodal image-tabular methods. The approaches typically rely on fusing embeddings extracted from an image encoder and a separate tabular encoder [3, 8, 9, 26, 28, 31, 34]. A different type of approach was presented in CHARMS [19], where tabular data is only used at the training stage for selective knowledge transfer to allow image-only inference; and

1) Contrastive Pretraining



2) Downstream Task Tuning

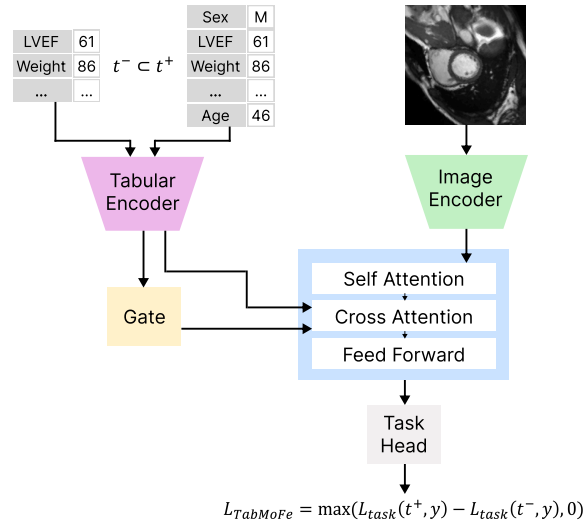


Figure 2. Overview of RoVTL. Our proposed framework, is composed of two main components: contrastive pretraining and downstream task tuning. In the pretraining stage, we introduce a novel tabular data missingness augmentation strategy, where random tabular entries are dropped (red cross) to teach the encoder to handle missing entries. During downstream task tuning, two subsets of the tabular attributes t are used as input into the encoder and ranked by the proposed TabMoFe loss. Further, our multimodal fusion module weights the importance of the tabular data for the multimodal fusion. Not illustrated in the figure is DGL [30], which is integrated into our fine-tuning pipeline.

in STiL [7], where semi-supervised learning is applied for image-tabular classification.

Pretraining-based Approaches. Multimodal self-supervised learning has achieved success in domains such as vision and language, as exemplified by CLIP [25]. Similar pretraining strategies have been applied to image-tabular data learning. MMCL [13] was the first to use contrastive learning for image-tabular data, using both modalities for the pretraining to achieve a powerful unimodal, image-only, inference. A similar approach was presented in TGV [15], where tabular data similarity is used to guide the pair sampling process in contrastive learning. TIP [6] was the first to use self-supervised pretraining for both image and tabular data inference, taking into consideration the missing values issue. However, TIP was not evaluated on the image-only edge case. Consequently, existing methods remain specialized either for image-only inference (MMCL, TGV) or joint image-tabular inference (TIP), with no model performing well in both scenarios. To bridge this divide, we introduce RoVTL, designed to handle the full spectrum of tabular data availability while maintaining strong image-only performance.

3. Methodology

3.1. Problem Definition

We consider a dataset consisting of image-tabular data pairs $\mathcal{D} = \{\{i, t\}_j, y_j\}_{j=1}^N$, where $\{i, t\}_j \in \mathcal{X}$ stand for the j -th

image and tabular sample, respectively. Each tabular sample t_j may include a variable number of available attributes. The corresponding label $y_j \in \mathcal{Y}$ can represent either a categorical class (for classification tasks) or a continuous value (for regression tasks). We aim to find a mapping $f : \mathcal{X} \rightarrow \mathcal{Y}$ from the input space to the label space that remains robust to varying numbers of tabular attributes at inference, including the case where tabular attributes are completely missing.

3.2. Method Overview

RoVTL is organized into two main stages, as shown in Fig. 2. First, we perform contrastive pretraining by contrasting images with varying subsets of tabular attributes, a key aspect of our approach that enables the model to learn robust representations under different degrees of missingness. Second, we fine-tune the pretrained encoders for downstream tasks. For this, we employ a multimodal fusion module based on gated cross-attention, where the gate adaptively weights the contribution of tabular features. To improve robustness to missing entries, we employ the proposed TabMoFe loss, and to ensure effective optimization of both encoders, we use DGL [30].

3.3. Pretraining with Missingness Simulation

The first step of RoVTL, multimodal contrastive pretraining, follows the basic setting of CLIP [25]. Specifically, it uses two modality specific encoders, an image encoder E_i and a tabular encoder E_t , that are followed by projection

heads f_i and f_t . For each image-tabular pair, we first apply augmentations to obtain \tilde{i} and \tilde{t} . The augmented inputs are encoded by the respective encoders to produce embeddings $v_i = E_i(\tilde{i}), v_i \in \mathbb{R}^{d_i}$ and $v_t = E_t(\tilde{t}), v_t \in \mathbb{R}^{d_t}$. These embeddings are then passed through the projection heads to obtain the projections $z_i = f_i(v_i), z_i \in \mathbb{R}^p$ and $z_t = f_t(v_t), z_t \in \mathbb{R}^p$ that are used for the contrastive loss.

While inspired by MMCL [13], our contrastive setting introduces a key difference: a novel approach to augmenting tabular data. Instead of corrupting attributes by replacing them with values observed elsewhere in the dataset, we leverage the common challenge of missing entries in tabular data as an augmentation strategy: given a sample’s full set of tabular attributes t^{full} with N_{full} entries, we randomly select a subset $t^{sub} \subseteq t^{full}$, where the size of t^{sub} is $[1, N_{full}]$, to serve as the input at each step, effectively simulating random entry missingness. This approach serves as a regularization technique that encourages the tabular encoder to learn meaningful representations even when only partial attributes are available.

4. Combining Imaging and Tabular Features

After pretraining, the learned encoders are fine-tuned for downstream tasks. To generate multimodal embeddings, we employ a gated image-tabular fusion module. Since tabular attributes can vary in size and importance across samples, their embeddings can differ substantially in the amount of information they carry. To adapt to this variability, we include a gating module, which allows the model to dynamically adjust the extent to which tabular inputs contribute to the multimodal embeddings. Formally, we extract the image and tabular features v_i and v_t from the pretrained encoders E_i and E_t . The embeddings are then projected into a shared latent space of dimension d via linear layers to obtain \tilde{v}_i and \tilde{v}_t . The generated image embeddings \tilde{v}_i are processed by a multi-head self-attention block to capture the intra-image dependencies,

$$\hat{v}_i = \text{SelfAttention}(\tilde{v}_i) \quad (1)$$

Next, cross-attention is applied from the image tokens \hat{v}_i to the tabular tokens \tilde{v}_t , where the image tokens serve as queries and the tabular tokens as keys and values. The [CLS] token from the tabular embedding \tilde{v}_t is passed through a gating module implemented as a multilayer perceptron (MLP) with a final sigmoid activation, producing a weight scalar $w \in [0, 1]$. The final multimodal embedding is then computed as,

$$v_m = \hat{v}_i + w \odot \text{CrossAttention}(\hat{v}_i, \tilde{v}_t) \quad (2)$$

This multimodal representation is then passed through a feed-forward layer before being used by the downstream task heads for predictions.

4.1. Tabular More vs. Fewer Loss

We extend the use of value missingness as a training-enhancement technique from pretraining to downstream task tuning. In contrast to other modalities, such as images or text, which can be defined as either present or absent, tabular data can have a variable number of attributes, making the notion of “missingness” more nuanced. Thus, applying modality missingness aware loss functions to tabular data requires specific adaptations.

We introduce TabMoFe loss, an adaptation to the SimMLM’s [22] MoFe loss. MoFe encourages the model to achieve better performance when more modalities are available. We follow this notion, but instead of comparing modalities, the loss is designed such that the ranking is based on the number of given tabular attributes. That is, at each iteration we sample two sets of tabular attributes, t^+ and t^- . As different attributes carry different weights for the output, some being more important than others, we ensure that $t^- \subset t^+ \subseteq t^{full}$. Further, the number of attributes in t^+ is in range $[1, N_a]$, where N_a represents the maximum amount of tabular attributes available, and t^- is in range $[0, N_t]$, where N_t is the number of attributes in t^+ . Given this setting, we can assume that the performance of the model with t^+ should be better or equal to that of t^- as it should not perform worse when more tabular attributes are available. Given this, we define the TabMoFe loss as,

$$\mathcal{L}_{TabMoFe} = \max(\mathcal{L}_{task}(i, t^+) - \mathcal{L}_{task}(i, t^-), 0) \quad (3)$$

Then, the full multimodal task loss is defined as,

$$\mathcal{L}_{multi} = \mathcal{L}_{task}(i, t^+) + \mathcal{L}_{task}(i, t^-) + \lambda \mathcal{L}_{TabMoFe} \quad (4)$$

where λ is introduced as a weighting factor.

4.2. Tuning with Disentangled Gradient Learning

A common challenge in multimodal learning is under-optimization, where joint training can lead to lower performance compared to unimodal models. One of the techniques addressing this issue is DGL [30]. We introduce this training strategy into our downstream task learning to ensure effective optimization of the unimodal models and the multimodal fusion module.

DGL explicitly decouples the optimization of modality encoders from that of the multimodal fusion module using two backward passes. In the first pass, a unimodal loss is computed for each modality, where separate task heads are attached to modality encoders,

$$\mathcal{L}_{unimodal} = \mathcal{L}_{task}(i) + \mathcal{L}_{task}(t) \quad (5)$$

This unimodal loss is used to update each modality encoder independently. The gradients that accumulate on the multimodal fusion parameters during this step are removed, and

the modality features are detached so that the upcoming multimodal loss does not propagate through them. In the second pass, the multimodal loss \mathcal{L}_{multi} is computed and backpropagated only through the multimodal fusion module. This disentanglement resolves the gradient interference between unimodal and multimodal objectives, ensuring stable and balanced optimization across modalities.

5. Experimental Setting

5.1. Datasets

UK Biobank [27] is a large-scale population-based cohort study. In this work, we use a subset of the biobank data consisting of pairs of short-axis cine Cardiac Magnetic Resonance (CMR) scans and tabular information incorporating attributes describing the demographics, lifestyle, and patient phenotype, among others. We use 39,975 pairs for training, 2,794 for validation, and 6,968 for testing. Our preprocessed CMR scans consist of 11 slices over 10 frames (sampled uniformly from the initial 50). The scans are cropped around the center of the heart to a size of 128×128 . Our tabular data consists of 129 attributes total, which include information such as sex, smoking status, or age. A full table representing all the used attributes and for which part of training they were used is available in Supplementary Material (SM) Table 5.

For the classification prediction target we use coronary artery disease (CAD) diagnosis based on the International Classification of Diseases (ICD10) codes, following the definitions in [13]. For a full list of the codes see SM Sec. H.2. As CAD is underrepresented in the dataset (only 8% of the volunteer subjects have CAD) we prepare a disease balanced subsample of size 6,426 for the downstream task fine-tuning. The subsample is designed such that 50% of the data is CAD positive and 50% is CAD negative. We only consider the diagnosis reported before the scan as positive label. The second evaluation task is regression of body mass index (BMI), a continuous variable whose prediction benefits from tabular data. For the fine-tuning of the task we assemble a subsample of 5,000 image-tabular data pairs. The validation and test set are unaltered.

M&Ms is a multi-centre, multi-vendor, and multi-disease dataset from a cardiac image segmentation challenge [4] used as an external dataset to evaluate whether our method can generalize to cardiac data outside the UK Biobank. It consists of 150 training, 32 validation, and 106 testing short-axis cine CMR images coming from 5 different centers and 4 different vendors. The dataset also includes tabular attributes describing the patient phenotype and demographics, a full list is available in SM Table 6. We perform the same sampling of the volumes as for the UK Biobank, using 11 image slices over 10 frames, cropped around the center of the heart to a size of 128×128 . We use the dataset for cardiac disease

classification, representing 4 different cardiac diseases and healthy samples.

Data Visual Marketing (DVM) dataset includes 1,451,784 images of cars at varying degree angles and their corresponding tabular attributes. We use the same preprocessing technique as [13], resulting in 70,565 training image-tabular pairs, 17,642 validation pairs, and 88,207 test pairs. The tabular attributes include fields on the cars’ length, height, or price. We evaluate the performance of our models on this dataset using model classification into 286 classes. As some of the attributes used in the pretraining can be used to directly identify the car model, such as the size of the car, we use a selection of attributes for the task tuning that ensures no information leakage between the training and test set. A full list of attributes used for the pretraining and fine-tuning is available in SM Table 7.

5.2. Implementation Details

All imaging encoders are based on the ResNet-50 [16] architecture, with a 3D version [14] used for the UK Biobank and 2D for DVM. The embedding size is set to 2048. For the tabular modality, we employ TARTE [20] as the encoder, initialized with its publicly released pretrained weights, with an embedding size of 768. The contrastive pretraining of RoVTL is implemented using Matryoshka Representation Learning [21], following TARTE with the projection head sizes of $\{64, 128, 256, 512, 768\}$. The comparing self-supervised pretraining methods are trained using their proposed settings, with a single projection head of size 128. The loss weighting parameter λ (Eq. 4) is empirically set to 0.05 for regression and 1 for classification. We train and fine-tune the models for 100 epochs on UK Biobank and 500 epochs on DVM. The projection heads are removed for the fine-tuning. For further implementation details for RoVTL and the comparison models, see SM Sec. I.

6. Results

6.1. Performance Comparison

We compare RoVTL against nine baseline methods, encompassing both end-to-end supervised and pretraining-based approaches. The supervised methods include Interact Fuse (IF) [8] and DAFT [31], while the pretraining-based methods comprise TGV [15] and MMCL [13], which perform image-tabular pretraining followed by image-only inference. In contrast, MaxFuse (MF) [28], ConcatFuse (CF) [26], and TIP [6] leverage both image and tabular embeddings during inference. For CF and MF we use our pretrained imaging and tabular encoders, while using the multimodal fusions from their respective papers. Additionally, CF* and MF* denote variants trained under our proposed downstream task fine-tuning setting, incorporating TabMoFe and DGL, to evaluate the transferability of our training strategy to differ-

Table 1. Performance comparison of RoVTL against baseline methods on UK Biobank CAD multilabel classification (AUC \uparrow), BMI regression (MAE \downarrow), and DVM car model multiclass classification (accuracy \uparrow). The performance is reported as a mean over tabular data incompleteness variants (0% - 100%). \ast : frozen backbones, $\text{\textcircled{f}}$: trainable backbones.

	UK Biobank				DVM	
	CAD \uparrow		BMI \downarrow		Car Model \uparrow	
	\ast	$\text{\textcircled{f}}$	\ast	$\text{\textcircled{f}}$	\ast	$\text{\textcircled{f}}$
<i>1) End-to-End Methods</i>						
Interact Fuse [8]	-	61.46	-	2.88	-	12.12
DAFT [31]	-	68.59	-	2.41	-	42.83
<i>2) Image-Tabular Pretraining-based Methods</i>						
<i>Image Only Inference</i>						
MMCL [13]	73.52	75.43	2.24	2.22	91.64	94.06
TGV [15]	73.22	76.78	2.52	2.28	92.52	94.23
<i>Image-Tabular Inference</i>						
Max Fuse [28]	74.45	81.38	2.91	1.60	90.14	86.05
Max Fuse* [28]	77.61	82.90	1.91	1.59	94.25	94.65
Concat Fuse [26]	75.13	76.33	3.05	1.77	90.02	86.37
Concat Fuse* [26]	76.10	82.90	2.01	1.79	93.57	94.32
TIP [6]	78.08	80.49	2.16	2.13	94.73	95.31
RoVTL (Ours)	84.68	84.91	1.51	1.69	94.10	96.11

Table 2. Evaluation of different tabular data augmentation techniques for image-tabular pretraining. CAD is evaluated using AUC (\uparrow), and LVEF using MAE (\downarrow). \ast : frozen backbones, $\text{\textcircled{f}}$: trainable backbones.

	<i>Image-Tabular</i>		<i>Image Only</i>	
	CAD \uparrow		LVEF \downarrow	
	\ast	$\text{\textcircled{f}}$	\ast	$\text{\textcircled{f}}$
w/o Augmentations	83.49	83.44	3.13	3.01
Corrupted (MMCL [13])	81.07	83.59	3.26	2.99
Missing (Ours)	84.68	84.91	3.09	2.99

ent networks. We evaluate all methods on two datasets, UK Biobank [27], where we perform multi-label CAD classification and BMI regression, and DVM car advertisement dataset [18], used for multi-class car model classification. Each model is trained in two configurations: trainable, where backbone weights are updated, and frozen, where backbones remain fixed. We report method performance as the average across varying levels of available tabular data (0%, 10%, 20%, ..., 100%), unless otherwise specified.

Table 1 shows the results of RoVTL compared with all baselines. For CAD classification, RoVTL consistently outperforms all other methods under both frozen and trainable configurations, surpassing TIP [6] by 4.6% in the frozen setting and 4.42% in the training setting. This improvement clearly demonstrates the benefit of incorporating robustness to missing entries during both pretraining and fine-tuning, unlike TIP, which only considers missingness during pretraining. Furthermore, CF* and MF* outperform their standard counterparts, proving the effectiveness of our downstream

task tuning pipeline and showing that it is transferable to different networks and tuning methods. Similar trends are visible for BMI regression, showing our method can generalize to other tasks. While in case of BMI regression MF* achieves the best performance under the trainable backbones setting, the performance of our method under the frozen setting is still the best overall. This behavior suggests the tasks particularly benefits from our pretraining strategy.

Lastly, to show that our method can generalize to 2D natural images, we evaluated it on the DVM car dataset for car model prediction. RoVTL outperforms the other baselines, showing that the framework can be also be applied to non-medical domain 2D imaging data without any adaptations. Notably, UK Biobank predictions involve over 80 attributes, compared to only 10 in DVM. While the relative improvement of RoVTL is more notable in the UK Biobank, it still benefits DVM, demonstrating the model’s robustness even with a small tabular attribute set.

6.2. Robustness to Missing Entries

The main objective of our framework is to ensure robust performance across different tabular data missingness scenarios, ranging from cases where no attributes are available to those where all are. We visualize the performance of our method and the best performing image-tabular baselines, TIP [6], CF* [26], and MF* [28], and image-only TGV [15] in Fig. 3. The performance of the other methods can be found in SM Section J.1. We show the performance under three different tabular data missingness scenarios: random value, least important (LI) attributes, and most important (MI) attributes. The LI and MI attributes are determined using random forest

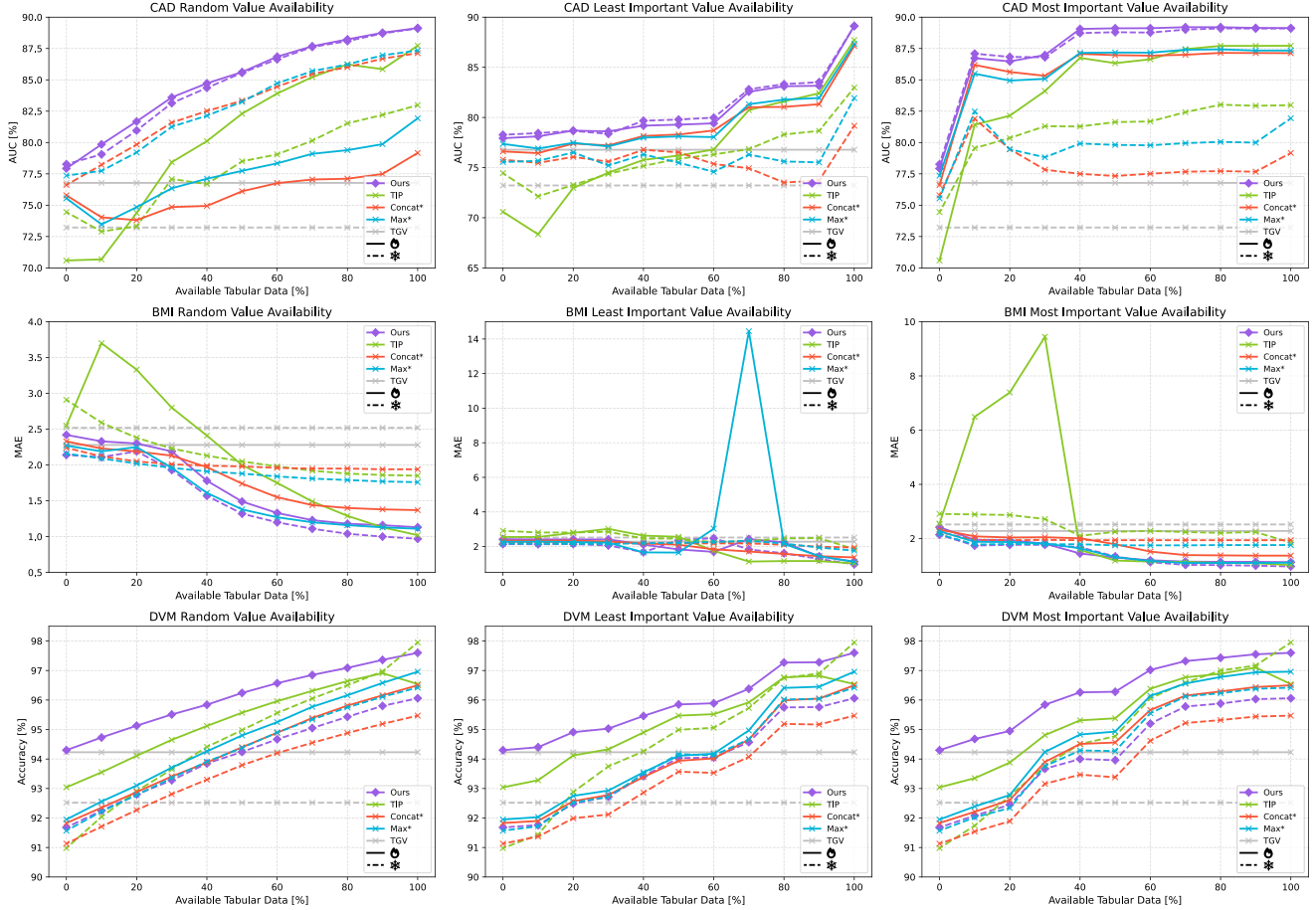


Figure 3. Model performance under different data availability scenarios from 0% to 100% tabular data used as input. CAD is evaluated using AUC (\uparrow), BMI using MAE (\downarrow), and DVM model classification using accuracy (\uparrow). \ast : frozen backbones, \bullet : trainable backbones.

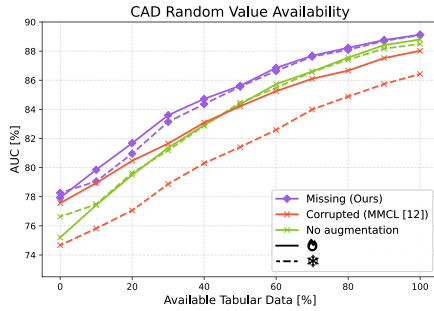


Figure 4. The effect of different tabular augmentation techniques used at pretraining on the result of CAD classification under random value missingness. \ast : frozen, \bullet : trainable backbones.

classifiers and regressors [23], following [6]. While these attributes may not fully reflect each model’s notion of importance, this approach standardizes features across methods for fair comparison. An analysis of RoVTL’s most important tabular attributes is provided in SM Section J.2. RoVTL

shows robustness to different tabular data missingness scenarios, achieving a high image-only performance that further improves with the addition of tabular data. Furthermore, the biggest performance difference between RoVTL and TIP [6] occurs when little to no tabular data is available, once again showing the importance of incorporating data missingness strategies not only at pretraining, but also at downstream task tuning.

6.3. Missingness as an Augmentation Technique

To prepare our tabular encoder for handling missing tabular entries, we introduce simulating tabular data missingness as an augmentation technique for the pretraining. We compare the proposed missingness augmentation to the tabular data corruption technique implemented in MMCL [13] and no tabular augmentations. The results are presented in Table 2. TARTE [20] is used as a tabular encoder for all the techniques. We evaluate the performance of the acquired backbones on CAD classification with both image and tabular data and for left ventricular ejection fraction (LVEF)

Table 3. The results on the multiclass cardiac disease classification on an external cardiac dataset called M&M’s [4]. The results are reported using AUC. ❄️: frozen, 🔥: trainable backbones.

	Disease Classification ↑	
	❄️	🔥
Interact Fuse [8]	-	62.63
DAFT [31]	-	57.45
MMCL [13]	64.93	65.37
TGV [15]	51.59	63.01
RoVTL (w/o pretraining)	-	66.50
RoVTL (Ours)	76.43	77.56

regression using images only. The analysis using multimodal and unimodal tasks allows us to understand whether exposing the tabular encoder to value missingness could have a negative impact on the image encoder. LVEF, being image-derived, does not require tabular data for prediction and thus serves as an ideal target for our experiment. The model pretrained using our augmentation strategy achieves the best performance for both tasks under both frozen and trainable settings. Higher improvement is observed in the image-tabular setting, and Fig. 4 shows that our augmentation technique is particularly helpful when only low amounts of tabular data are available. While the performance improvement is not as significant for image-only setting, we note that our augmentation technique allows to keep high unimodal performance while obtaining a tabular encoder robust to missing values.

6.4. Image-Tabular Pretraining Generalizability

Development of tabular foundation models such as TARTE [20] can pave the way for multimodal vision-tabular models. We explore the potential of this idea by evaluating our vision and tabular encoders pretrained on the UK Biobank [27] dataset on an external cardiac dataset, M&M’s [4], for the task of cardiac disease classification. Due to the rigid design of the tabular encoder in TIP [6] we are unable to use TIP’s pretrained encoders for the comparison. Thus, we evaluate RoVTL against image-only inference methods such as MMCL [13] and TGV [15], end-to-end supervised methods such as IF [8] and DAFT [31], and a randomly initialized variant of our model. The results are reported as mean AUC over the varying tabular data missingness scenarios. The results are presented in Table 3. RoVTL achieves the best performance, outperforming the randomly initialized model by 9.93% with frozen backbones and 11.06% with trainable backbone. These results highlight RoVTL’s generalization ability and underscore its potential as a foundation for developing large-scale medical tabular-vision models.

Table 4. Ablation study showing the effectiveness of each part of our method. CAD is evaluated using AUC, while BMI using MAE. ❄️: frozen backbones, 🔥: trainable backbones.

	CAD ↑		BMI ↓	
	❄️	🔥	❄️	🔥
w/o pretraining	-	82.94	-	1.71
w/o gate	84.60	82.13	1.61	1.87
w/o downstream missingness	77.07	83.37	4.64	4.53
w/o TabMoFe	84.19	83.09	1.54	1.98
w/o DGL	84.40	84.47	1.87	1.98
RoVTL (Ours)	84.68	84.91	1.51	1.69

6.5. Ablation Study

Each element of our method was designed to ensure robustness to missing tabular data entries. To assess the contribution of each element, we conduct an ablation study, with results summarized in Table 4. We use multilabel CAD classification and BMI regression for the ablations. RoVTL with all its components achieves the best results for all the tasks under both frozen and trainable backbones, clearly showing the effectiveness of our method. In addition, our proposed attribute missingness augmentation has the biggest impact in performance, demonstrating the importance of training under diverse tabular data availability scenarios.

7. Conclusion

We introduce RoVTL: Robust Vision-Tabular Learning, the first vision-tabular method, to the best of our knowledge, that performs effectively across the full spectrum of tabular data completeness. RoVTL consists of two main components, contrastive pretraining and downstream task tuning. At pretraining, we propose to leverage tabular data missingness as an augmentation strategy, simulating incomplete entries to enhance the robustness of the tabular encoder. During downstream task tuning, RoVTL uses a gated cross-attention module to adaptively weight tabular data in the multimodal embedding. Robustness is further enhanced with TabMoFe loss, which ranks performance based on available tabular attributes, and disentangled gradient learning ensures effective optimization of both image and tabular encoders. Our extensive experiments demonstrate that RoVTL outperforms prior methods, with the largest gains when tabular data is limited. Successful evaluation on external medical datasets highlights its potential for vision-tabular foundation models, while results on the 2D car dataset demonstrate its generalizability to multiple domains. Overall, RoVTL provides a generalizable and robust solution for vision-tabular learning, bridging the gap between image-only and multimodal inference and demonstrating effectiveness across the full spectrum of tabular data scenarios.

References

- [1] Muhammad Awais, Muzammal Naseer, Salman Khan, Rao Muhammad Anwer, Hisham Cholakkal, Mubarak Shah, Ming-Hsuan Yang, and Fahad Shahbaz Khan. Foundation models defining a new era in vision: a survey and outlook. *IEEE Transactions on Pattern Analysis and Machine Intelligence*, 2025. 2
- [2] Wenjia Bai, Matthew Sinclair, Giacomo Tarroni, Ozan Oktay, Martin Rajchl, Ghislain Vaillant, Aaron M Lee, Nay Aung, Elena Lukaschuk, Mihir M Sanghvi, et al. Automated cardiovascular magnetic resonance image analysis with fully convolutional networks. *Journal of cardiovascular magnetic resonance*, 20(1):65, 2018. 1
- [3] Balázs Borsos, Corinne G Allaart, and Aart van Halteren. Predicting stroke outcome: a case for multimodal deep learning methods with tabular and ct perfusion data. *Artificial Intelligence in Medicine*, 147:102719, 2024. 2
- [4] Victor M Campello, Polyxeni Gkontra, Cristian Izquierdo, Carlos Martin-Isla, Alireza Sojoudi, Peter M Full, Klaus Maier-Hein, Yao Zhang, Zhiqiang He, Jun Ma, et al. Multi-centre, multi-vendor and multi-disease cardiac segmentation: the m&ms challenge. *IEEE Transactions on Medical Imaging*, 40(12):3543–3554, 2021. 2, 5, 8, 1, 3
- [5] Tianqi Chen and Carlos Guestrin. Xgboost: A scalable tree boosting system. In *Proceedings of the 22nd acm sigkdd international conference on knowledge discovery and data mining*, pages 785–794, 2016. 2
- [6] Siyi Du, Shaoming Zheng, Yinsong Wang, Wenjia Bai, Declan P O’Regan, and Chen Qin. Tip: Tabular-image pre-training for multimodal classification with incomplete data. In *European Conference on Computer Vision*, pages 478–496. Springer, 2024. 1, 3, 5, 6, 7, 8
- [7] Siyi Du, Xinzhe Luo, Declan P O’Regan, and Chen Qin. Stil: Semi-supervised tabular-image learning for comprehensive task-relevant information exploration in multimodal classification. In *Proceedings of the Computer Vision and Pattern Recognition Conference*, pages 15549–15559, 2025. 3
- [8] Hongyi Duanmu, Pauline Boning Huang, Srinidhi Brahmaravar, Stephanie Lin, Thomas Ren, Jun Kong, Fusheng Wang, and Tim Q Duong. Prediction of pathological complete response to neoadjuvant chemotherapy in breast cancer using deep learning with integrative imaging, molecular and demographic data. In *International conference on medical image computing and computer-assisted intervention*, pages 242–252. Springer, 2020. 2, 5, 6, 8, 1
- [9] Daniel Duenias, Brennan Nichyporuk, Tal Arbel, Tammy Riklin Raviv, et al. Hyperfusion: A hypernetwork approach to multimodal integration of tabular and medical imaging data for predictive modeling. *Medical Image Analysis*, 102:103503, 2025. 2
- [10] David C Dugdale, Ronald Epstein, and Steven Z Pantilat. Time and the patient–physician relationship. *Journal of general internal medicine*, 14(Suppl 1):S34, 1999. 1
- [11] German National Cohort (GNC) Consortium geschaeftsstelle@ nationale-kohorte. de. The german national cohort: aims, study design and organization. *European journal of epidemiology*, 29(5):371–382, 2014. 1
- [12] Léo Grinsztajn, Edouard Oyallon, and Gaël Varoquaux. Why do tree-based models still outperform deep learning on typical tabular data? *Advances in neural information processing systems*, 35:507–520, 2022. 2
- [13] Paul Hager, Martin J Menten, and Daniel Rueckert. Best of both worlds: Multimodal contrastive learning with tabular and imaging data. In *Proceedings of the IEEE/CVF Conference on Computer Vision and Pattern Recognition*, pages 23924–23935, 2023. 1, 3, 4, 5, 6, 7, 8
- [14] Kensho Hara, Hirokatsu Kataoka, and Yutaka Satoh. Can spatiotemporal 3d cnns retrace the history of 2d cnns and imagenet? In *Proceedings of the IEEE conference on Computer Vision and Pattern Recognition*, pages 6546–6555, 2018. 5
- [15] Marta Hasny, Maxime Di Folco, Keno Bresssem, and Julia Schnabel. Tables guide vision: Learning to see the heart through tabular data. *arXiv preprint arXiv:2503.14998*, 2025. 1, 3, 5, 6, 8
- [16] Kaiming He, Xiangyu Zhang, Shaoqing Ren, and Jian Sun. Deep residual learning for image recognition. In *Proceedings of the IEEE conference on computer vision and pattern recognition*, pages 770–778, 2016. 5
- [17] Noah Hollmann, Samuel Müller, Katharina Eggenberger, and Frank Hutter. TabPFN: A transformer that solves small tabular classification problems in a second. *arXiv preprint arXiv:2207.01848*, 2022. 2
- [18] Jingmin Huang, Bowei Chen, Lan Luo, Shigang Yue, and Iadh Ounis. Dvm-car: A large-scale automotive dataset for visual marketing research and applications, 2023. 2, 6, 1, 3
- [19] Jun-Peng Jiang, Han-Jia Ye, Leye Wang, Yang Yang, Yuan Jiang, and De-Chuan Zhan. Tabular insights, visual impacts: transferring expertise from tables to images. In *Forty-first International Conference on Machine Learning*, 2024. 2
- [20] Myung Jun Kim, Félix Lefebvre, Gaëtan Brison, Alexandre Perez-Lebel, and Gaël Varoquaux. Table foundation models: on knowledge pre-training for tabular learning. *arXiv preprint arXiv:2505.14415*, 2025. 2, 5, 7, 8
- [21] Aditya Kusupati, Gantavya Bhatt, Aniket Rege, Matthew Wallingford, Aditya Sinha, Vivek Ramanujan, William Howard-Snyder, Kaifeng Chen, Sham Kakade, Prateek Jain, et al. Matryoshka representation learning. *Advances in Neural Information Processing Systems*, 35:30233–30249, 2022. 5
- [22] Sijie Li, Chen Chen, and Jungong Han. Simmlm: A simple framework for multi-modal learning with missing modality. *arXiv preprint arXiv:2507.19264*, 2025. 2, 4
- [23] Andy Liaw, Matthew Wiener, et al. Classification and regression by randomforest. *R news*, 2(3):18–22, 2002. 7
- [24] Jingang Qu, David Holzmüller, Gaël Varoquaux, and Marine Le Morvan. Tabicl: A tabular foundation model for in-context learning on large data. *arXiv preprint arXiv:2502.05564*, 2025. 2
- [25] Alec Radford, Jong Wook Kim, Chris Hallacy, Aditya Ramesh, Gabriel Goh, Sandhini Agarwal, Girish Sastry, Amanda Askell, Pamela Mishkin, Jack Clark, et al. Learning transferable visual models from natural language supervision. In *International conference on machine learning*, pages 8748–8763. PmLR, 2021. 3

- [26] Simeon Spasov, Luca Passamonti, Andrea Duggento, Pietro Lio, Nicola Toschi, Alzheimer’s Disease Neuroimaging Initiative, et al. A parameter-efficient deep learning approach to predict conversion from mild cognitive impairment to alzheimer’s disease. *Neuroimage*, 189:276–287, 2019. [2](#), [5](#), [6](#)
- [27] Cathie Sudlow, John Gallacher, Naomi Allen, Valerie Beral, Paul Burton, John Danesh, Paul Downey, Paul Elliott, Jane Green, Martin Landray, et al. Uk biobank: an open access resource for identifying the causes of a wide range of complex diseases of middle and old age. *PLoS medicine*, 12(3): e1001779, 2015. [1](#), [2](#), [5](#), [6](#), [8](#), [3](#)
- [28] Luís A Vale-Silva and Karl Rohr. Long-term cancer survival prediction using multimodal deep learning. *Scientific Reports*, 11(1):13505, 2021. [2](#), [5](#), [6](#)
- [29] Ashish Vaswani, Noam Shazeer, Niki Parmar, Jakob Uszkoreit, Llion Jones, Aidan N Gomez, Łukasz Kaiser, and Illia Polosukhin. Attention is all you need. *Advances in neural information processing systems*, 30, 2017. [2](#)
- [30] Shicai Wei, Chunbo Luo, and Yang Luo. Boosting multimodal learning via disentangled gradient learning. *arXiv preprint arXiv:2507.10213*, 2025. [2](#), [3](#), [4](#)
- [31] Tom Nuno Wolf, Sebastian Pölsterl, Christian Wachinger, Alzheimer’s Disease Neuroimaging Initiative, et al. Daft: A universal module to interweave tabular data and 3d images in cnns. *NeuroImage*, 260:119505, 2022. [2](#), [5](#), [6](#), [8](#), [1](#)
- [32] Han-Jia Ye, Si-Yang Liu, Hao-Run Cai, Qi-Le Zhou, and De-Chuan Zhan. A closer look at deep learning methods on tabular datasets. *arXiv preprint arXiv:2407.00956*, 2024. [2](#)
- [33] Wayne Xin Zhao, Kun Zhou, Junyi Li, Tianyi Tang, Xiaolei Wang, Yupeng Hou, Yingqian Min, Beichen Zhang, Junjie Zhang, Zican Dong, et al. A survey of large language models. *arXiv preprint arXiv:2303.18223*, 1(2), 2023. [2](#)
- [34] Hanci Zheng, Zongying Lin, Qizheng Zhou, Xingchen Peng, Jianghong Xiao, Chen Zu, Zhengyang Jiao, and Yan Wang. Multi-transsp: Multimodal transformer for survival prediction of nasopharyngeal carcinoma patients. In *International Conference on Medical Image Computing and Computer-Assisted Intervention*, pages 234–243. Springer, 2022. [2](#)

No Data? No Problem: Robust Vision-Tabular Learning with Missing Values

Supplementary Material

H. Detailed Data Description

H.1. Tabular Attributes

Selection of the tabular attributes in our method is dependent on the training stage. We present comprehensive overview of the attributes and at which stage they are used in Table 5 for UK Biobank [27], Table 6 for M&Ms [4], and Table 7 for DVM [18]. For the UK Biobank we also include the field IDs that are used to extract the attributes. The attributes that are marked as *extracted* are derived using automated cardiac MRI analysis [2].

H.2. ICD Codes

The labels for multilabel cardiovascular artery disease (CAD) classification task are defined using the ICD-10 codes of categories I20-I25. Diseases defined by the following codes are used as positive labels:

- Angina pectoris: I200, I202, I208, I209;
- Myocardial infarction: I210, I211, I212, I213, I214, I219;
- Other acute ischemic heart disease: I240, I248, I249;
- Chronic ischemic heart disease: I250, I251, I252, I253, I254, I255, I256, I258, I259.

We extract the date of each MR scan and consider the subject CAD positive only if the disease was reported prior to the scanning date. UK Biobank uses self-reporting of diseases and due to the nature of CAD, which can remain undiagnosed for years, it is possible that some of the healthy subjects do have CAD. Addressing the label uncertainty in UK Biobank is left for future work.

H.3. M&M’s Cardiac Disease Classification

The cardiac diseases included in the M&M’s dataset [4] differ from those used for the CAD classification in UK Biobank [27]. M&M’s includes patients representing four cardiac diseases and healthy samples. The diseases are:

- Hypertrophic cardiomyopathy (HCM),
- Dilated cardiomyopathy (DCM),
- Hypertensive Heart Disease (HHD),
- Abnormal Right Ventricle (ARV).

I. Implementation Details

I.1. Image Augmentations

Image augmentations are applied using the torchvision library. Due to different data formats (2D vs. 3D) between DVM [18] and cardiac datasets, UK Biobank [27] and M&M’s [4], different augmentations are applied to them.

For UK biobank and M&M’s the following augmentations are applied:

- RandomHorizontalFlip(probability=0.5),
- RandomResizedCrop(size=128, scale=(0.6, 1.0)),
- RandomRotation(degrees=45).

For DVM the following image augmentations are used:

- ColorJitter(brightness=0.8, contrast=0.8, saturation=0.8, probability=0.8),
- RandomGrayscale(probability=0.2),
- GaussianBlur(kernel_size=29, sigma=(0.1, 2.0), probability=0.5),
- RandomResizedCrop(size=128, scale=(0.6, 1.0), ratio=(0.75, 1.33)),
- RandomHorizontalFlip(probability=0.5),

I.2. Tabular Data Augmentations

Tabular Data Corruption. In our pretraining experiments assessing the impact of different augmentation strategies, we adopt the tabular data corruption scheme as described in MMCL [13], using an augmentation rate of 0.3. In this scheme, randomly selected entries are replaced with alternative values drawn from the empirical marginal distribution of their respective columns, that is, values observed elsewhere in the dataset.

I.3. Baselines

For the baselines, we follow the settings and specifications provided by the original authors. Any details specific to our implementations are described below.

Supervised baselines. The end-to-end supervised baselines, which include Interact Fuse (IF) [8] and DAFT [31] are trained using the attributes as listed for each task in Tables 5- 7, without any pretraining including the remaining attributes. This approach ensures no leakage of task specific information, as pretraining incorporated attributes that are later used as labels for downstream tasks.

TIP [6]. The original TIP pipeline does not include pretraining with labels, which was introduced in MMCL [13]. To ensure proper comparison to other pretraining based approaches we use the same set of attributes, which also incorporate labels. For TIP, we use fixed masks at downstream task tuning that mask the attributes that should be excluded for the given downstream task prediction. As the TIP tabular encoder expects the attributes at certain order, we could not simply exclude the values and pad the remaining tokens, motivating the use of masking which was already implemented in the method as a way of marking missing entries. For

Table 5. Tabular attributes extracted from the UK Biobank [27] and their corresponding field IDs. The ✓ symbol in the CAD or BMI column indicates that the attribute is used in the respective downstream task, while the ✗ symbol indicates that it is excluded from that task. All listed attributes are used during pretraining.

Tabular Feature	Field ID	CAD	BMI	Tabular Feature	Field ID	CAD	BMI
Alcohol drinker status	20117	✓	✓	Alcohol intake frequency	1558	✓	✓
Pulse rate automated	102	✓	✓	Augmentation index for PWA	12681	✓	✓
Average heart rate	22426	✓	✓	Basal metabolic rate	23105	✓	✓
Medication for cholesterol, blood pressure or diabetes	6177	✓	✓	Body fat percentage	23099	✓	✓
Body mass index	21001	✓	✗	Body surface area	22427	✓	✓
Cardiac index	22425	✓	✓	Cardiac index during PWA	12702	✓	✓
Cardiac operations performed	20004	✓	✓	Cardiac output	22424	✓	✓
Cardiac output during PWA	12682	✓	✓	Central augmentation pressure during PWA	12680	✓	✓
Central pulse pressure during PWA	12678	✓	✓	Central systolic blood pressure during PWA	12677	✓	✓
Cholesterol lowering medication regularly taken	6177	✓	✓	Current tobacco smoking	1239	✓	✓
Diastolic blood pressure automated	4079	✓	✓	Diastolic blood pressure manual reading	94	✓	✓
Diastolic brachial blood pressure during PWA	12675	✓	✓	Duration of heavy DIY	2634	✓	✓
Duration of moderate activity	894	✓	✓	Duration of strenuous sports	10010	✓	✓
Duration of vigorous activity	914	✓	✓	Duration of walks	874	✓	✓
Duration walking for pleasure	981	✓	✓	End systolic pressure during PWA	12683	✓	✓
End systolic pressure index during PWA	12684	✓	✓	Ever smoked	20160	✓	✓
Exposure to tobacco smoke at home	1269	✓	✓	Exposure to tobacco smoke outside home	1279	✓	✓
Falls in the last year	2296	✓	✓	Frequency of other exercises in last 4 weeks	3637	✓	✓
Heart rate during PWA	12673	✓	✓	Height	12144	✓	✗
Hip circumference	49	✓	✓	Hormone replacement therapy medication regularly taken	6153	✓	✓
Mean arterial pressure during PWA	12687	✓	✓	Number of beats in waveform average for PWA	12679	✓	✓
Days/week moderate activity	884	✓	✓	Days/week vigorous activity	904	✓	✓
Days/week walked	864	✓	✓	Overall health rating	2178	✓	✓
P duration	12338	✓	✓	Pace	3079	✓	✓
Pack years adult smoking as proportion of lifespan exposed	20162	✓	✓	Pack years of smoking	20161	✓	✓
Past tobacco smoking	1249	✓	✓	Peripheral pulse pressure during PWA	12676	✓	✓
Pulse wave Arterial Stiffness index	21021	✓	✓	QRS duration	12340	✓	✓
Shortness of breath walking on level ground	4717	✓	✓	Sleep duration	1160	✓	✓
Sleeplessness / insomnia	1200	✓	✓	Smoking/smokers in household	1259	✓	✓
Stroke volume during PWA	12686	✓	✓	Systolic blood pressure	4080	✓	✓
Systolic brachial blood pressure during PWA	12674	✓	✓	Total mass	23283	✓	✓
Total peripheral resistance during PWA	12685	✓	✓	Ventricular rate	12336	✓	✓
Waist circumference	48	✓	✓	Weight	21002	✓	✗
Whole body fat-free mass	23101	✓	✓	Whole body fat mass	23100	✓	✓
Whole body water mass	23102	✓	✓	Worrier / anxious feelings	1980	✓	✓
Date of birth (Age)	33	✓	✓	Sex	31	✓	✓
Heart Failure (I50)	13135	✗	✗	Atrial Fibrillation and Flutter (I48)	13135	✗	✗
Nonrheumatic Aortic Valve Disorders (I25)	131324	✗	✗	Other Diseases of Pericardium (I31)	131316	✗	✗
Paroxysmal Tachycardia (I47)	131348	✗	✗	Acute Pericarditis (I30)	131314	✗	✗
Atrioventricular and Left Bundle-Branch Block (I44)	131342	✗	✗	Nonrheumatic Mitral Valve Disorders (I34)	131322	✗	✗
Acute and Subacute Endocarditis (I33)	131320	✗	✗	Other Cardiac Arrhythmias (I49)	131352	✗	✗
Cardiomyopathy (I42)	131338	✗	✗	Acute Myocarditis (I40)	131334	✗	✗
Other Conduction Disorders (I45)	131344	✗	✗	Cardiac Arrest (I46)	131346	✗	✗
Nonrheumatic Tricuspid Valve Disorders (I36)	131326	✗	✗	Essential (Primary) Hypertension (I10)	131286	✗	✗
Hypertensive Heart Disease (I11)	131288	✗	✗	Hypertensive Renal Disease (I12)	131290	✗	✗
Hypertensive Heart and Renal Disease (I13)	131292	✗	✗	Secondary Hypertension (I15)	131294	✗	✗
Insulin-Dependent Diabetes Mellitus (E10)	130706	✗	✗	Non-Insulin-Dependent Diabetes Mellitus (E11)	130708	✗	✗
Other Specified Diabetes Mellitus (E13)	130712	✗	✗	Unspecified Diabetes Mellitus (E14)	130714	✗	✗
Angina Pectoris (I20)	131296	✗	✗	Other Acute Ischaemic Heart Diseases (I24)	131304	✗	✗
Chronic Ischaemic Heart Disease (I25)	131306	✗	✗	Myocardial Infarction (I21)	42000	✗	✗
Left Ventricular Ejection Fraction	Extracted	✓	✓	Left Ventricular End-diastolic Volume	Extracted	✓	✓
Left Ventricular End-systolic Volume	Extracted	✓	✓	Left Ventricular Stroke Volume	Extracted	✓	✓
Left Ventricular End-diastolic Mass	Extracted	✓	✓	Left Ventricular Cardiac Output	Extracted	✓	✓
Right Ventricular End-diastolic Volume	Extracted	✓	✓	Right Ventricular End-systolic Volume	Extracted	✓	✓
Right Ventricular Stroke Volume	Extracted	✓	✓	Right Ventricular Ejection Fraction	Extracted	✓	✓
Right Ventricular Cardiac Output	Extracted	✓	✓	Myocardial End-diastolic Volume	Extracted	✓	✓
Myocardial End-diastolic Volume	Extracted	✓	✓	Myocardial End-systolic Volume	Extracted	✓	✓

the edge-case of tabular data being fully missing, we follow the typical TIP prediction pipeline, but mask all the tabular tokens.

Concat Fuse (CF) [26] and Max Fuse (MF) [28]. We use two different multimodal embedding concatenation methods as baselines. Namely, CF where tabular and image embeddings are concatenated together, and MF, where element-wise max pooling is performed across two embeddings, selecting the larger values in each feature dimension to form the multimodal embedding. To ensure proper comparison, we use our pretrained image and tabular encoders for the two concatenation approaches. Furthermore, we compare RoVTL against those methods tuned using our downstream task tuning approach and the standard setting, without incorporating TabMoFe loss, missing value simulation, and DGL [30].

Table 6. Full list of the tabular attributes from the M&M’s dataset [4]. All attributes listed are used for the downstream task (cardiac disease classification), as denoted by ✓.

Tabular Feature	Classification
Left Ventricular End-Diastolic Volume	✓
Left Ventricular End-Systolic Volume	✓
Left Ventricular Stroke Volume	✓
Left Ventricular Ejection Fraction	✓
Left Ventricular End-Diastolic Mass	✓
Left Ventricular Cardiac Output	✓
Right Ventricular End-Diastolic Volume	✓
Right Ventricular End-Systolic Volume	✓
Right Ventricular Stroke Volume	✓
Right Ventricular Ejection Fraction	✓
Right Ventricular Cardiac Output	✓
Myocardial End-Diastolic Volume	✓
Myocardial End-Systolic Volume	✓
Height	✓
Weight	✓
Sex	✓

I.4. Downstream Task Tuning

We perform downstream task tuning under two settings, with frozen and trainable backbones. The multimodal fusion module is trainable in every setting and is added on top of the pre-

Table 7. A list of tabular attributes from the DVM dataset [18]. All the attributes are used for the pretraining. The attributes denoted by ✓ in the *Classification* column are used in the downstream task prediction (car model classification), while the ones marked by ✗ are excluded.

Tabular Feature	Classification
Manufacturer Name	✗
Car Model	✗
Color	✓
Registration Year	✓
Body Type	✓
Mileage Miles	✓
Engine Size	✓
Gearbox	✓
Fuel Type	✓
Price	✓
Engine Power	✗
Annual Tax	✗
Wheelbase	✗
Length	✗
Height	✗
Width	✗
Average Miles per Gallon	✗
Top Speed	✗
Seat Count	✓
Door Count	✓

trained backbones. The Adam optimizer with a weight decay of $1e^{-4}$ and an effective batch size of 512 for DVM [18] and 256 for UK Biobank [27] is used. We perform a learning rate sweep covering four values, $\{1e^{-3}, 3e^{-3}, 1e^{-4}, \text{ and } 3e^{-4}\}$, with the best one selected based on the validation set results. The tuning is performed for 500 epochs for the DVM dataset, 100 for M&Ms dataset [4], and 100 for UK Biobank. We use the Huber loss for regression (BMI regression), Binary Cross Entropy with Logits loss for multilabel classification (DVM car model prediction and M&Ms cardiac disease prediction), and Cross Entropy loss for multiclass classification (CAD classification on UK Biobank). The augmentation rate is set to 0.95.

J. Additional Experiments

J.1. Robustness to Missing Entries (Complete)

We provide full results for robustness to missing entries in Fig. 5. For clarity, we omitted baselines with the lowest performance in the main body of the paper. RoVTL outperforms the other methods on all tasks. Furthermore, incorporating our downstream fine-tuning setting to CF and MF improves the robustness of both of the methods to limited tabular data regimes, further showing the strength of our introduced training pipeline.

J.2. Interpretability

We evaluate the tabular attributes attention scores to better understand which features RoVTL uses to make predictions. The results are shown in Fig. 6 for CAD classification, Fig. 7 for BMI regression, and in Fig. 8 for car model prediction. To obtain the attention scores, the raw attention scores are extracted from the final cross-attention layer. The attention weights assigned to each attribute are then aggregated by first taking the mean over across all heads and then over the image tokens, which produces a single score for each

tabular attribute. The aggregation is performed per class for classification and on full test set for regression. RoVTL takes advantage of the complementary information in the tabular attributes that is not directly visible on the image, such as the engine size or mileage of the car, to make predictions. For BMI regression, attributes describing the body, such as the whole body fat mass or whole body fat-free mass, are attended to the most. This behavior confirms that the model does not treat the tabular data as auxiliary, but instead learns to rely on tabular features that provide predictive value beyond what is visible in the images, resulting in more robust and interpretable multimodal predictions.

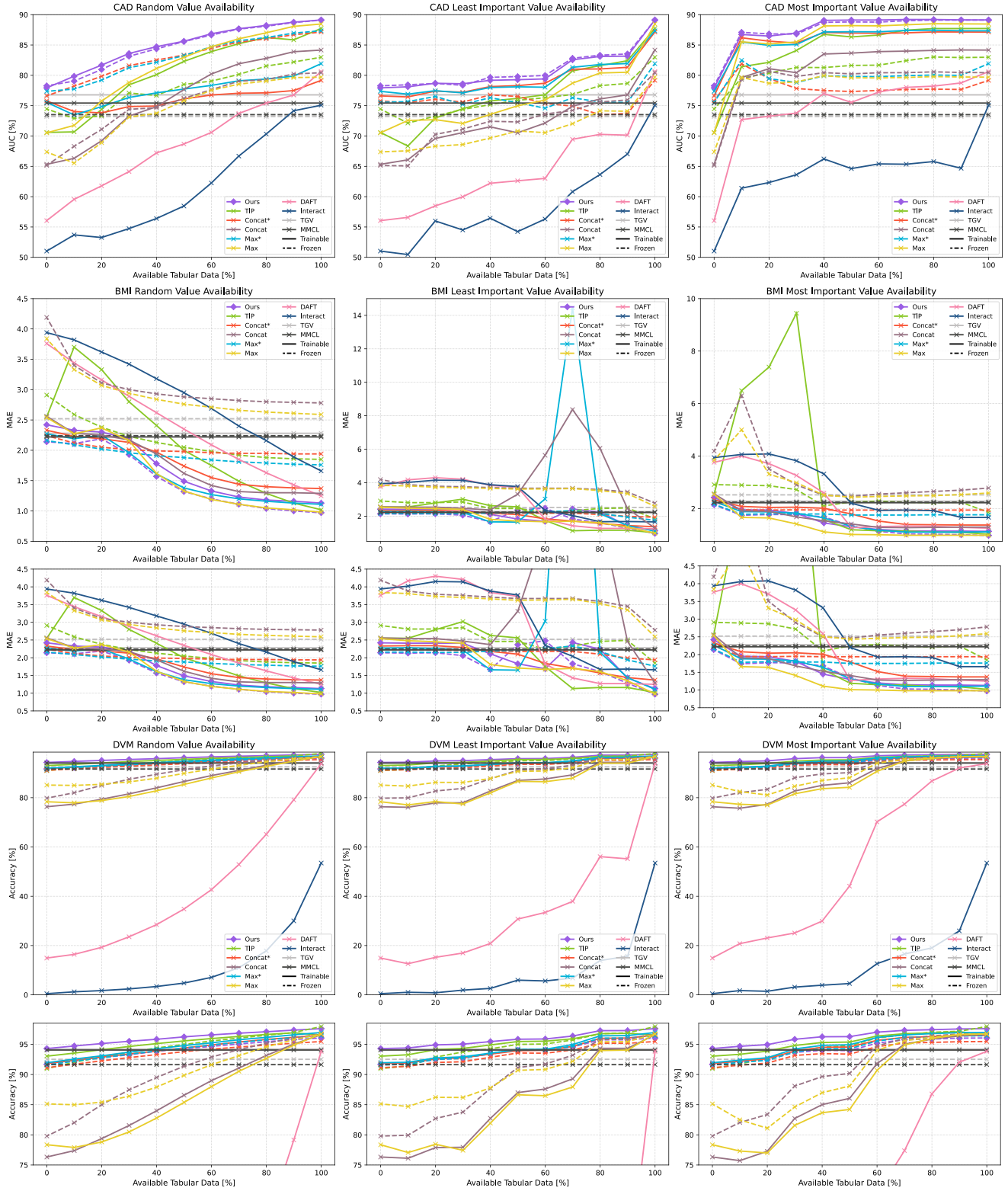


Figure 5. Model performance plotted over tabular data availability from 0% to 100%. CAD is reported using AUC (\uparrow), BMI using MAE (\downarrow), and DVM car classification using accuracy (\uparrow). For clarity, zoomed-in versions are provided for BMI regression and car model classification with DVM to highlight the performance differences between the models. \ast : frozen backbones, \bullet : trainable backbones.



Figure 6. Attention scores per attribute for CAD classification with the UK Biobank.

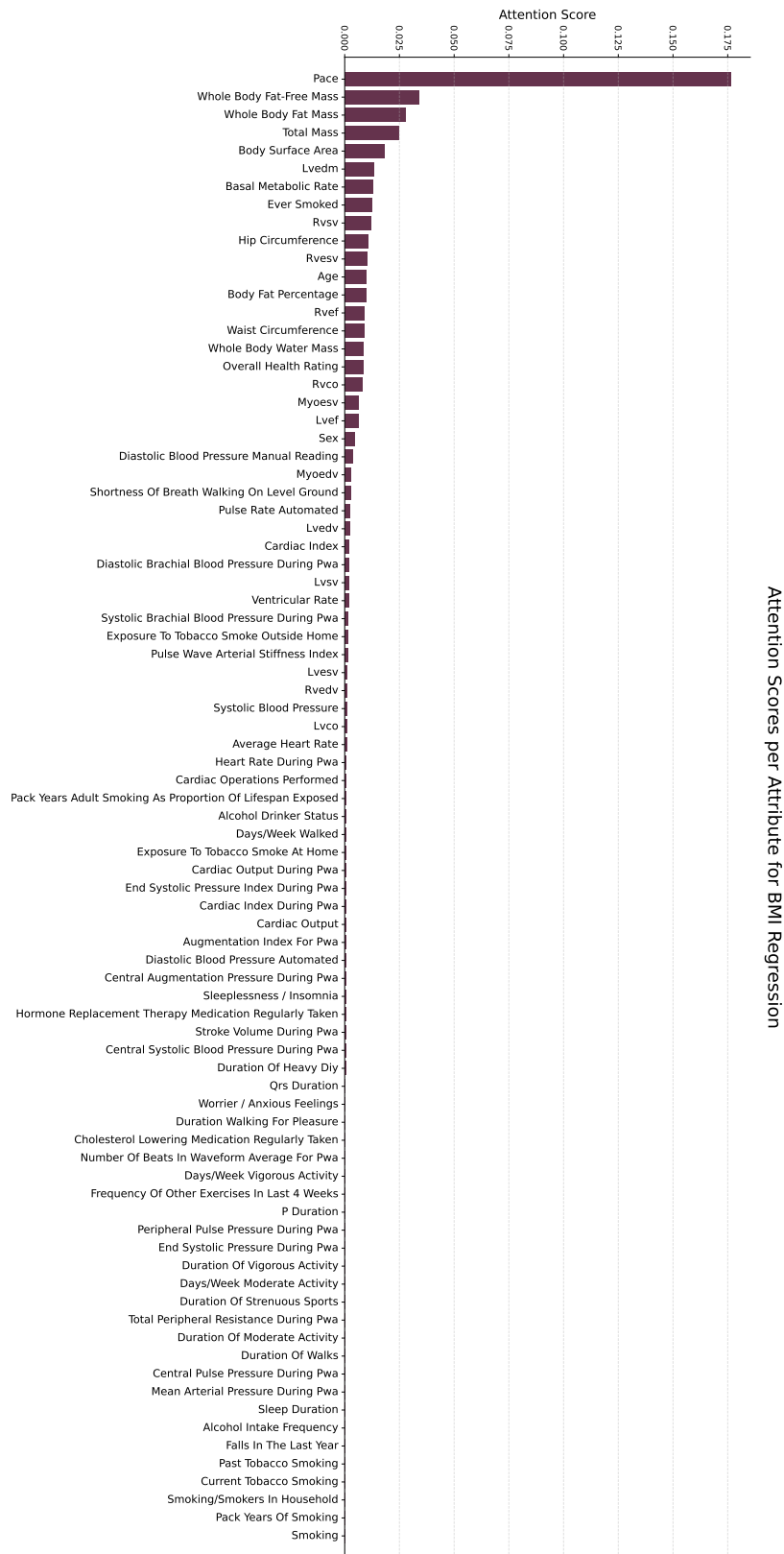


Figure 7. Attention scores per attribute for BMI regression with the UK Biobank.

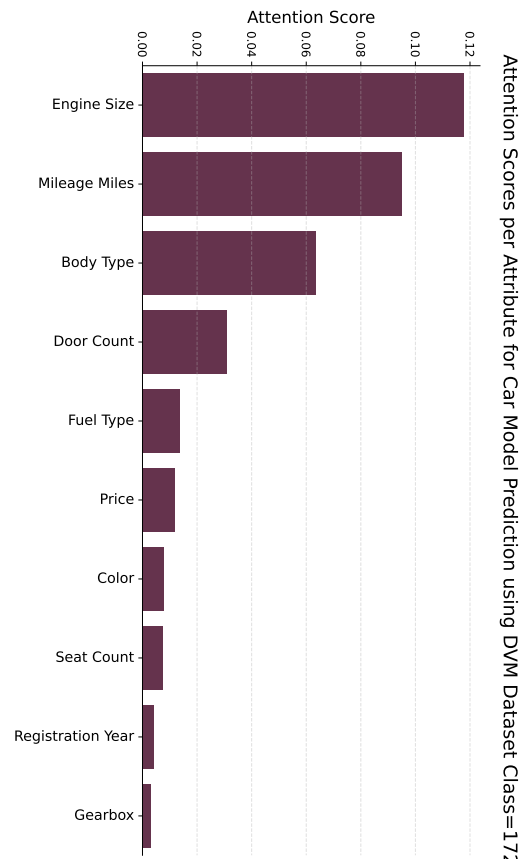


Figure 8. Attention scores per attribute for BMI regression with the UK Biobank.